Spectroscopic Investigation of Ni Speciation in Hardened Cement Paste

ARTICLE *in* ENVIRONMENTAL SCIENCE AND TECHNOLOGY · MAY 2006

Impact Factor: 5.33 · DOI: 10.1021/es052240q · Source: PubMed

Environ. Sci. Technol. **2006**, *40,* 2275−2282

Spectroscopic Investigation of Ni Speciation in Hardened Cement Paste

M. VESPA,*,†,‡ R. DÄHN,† D. GROLIMUND,† E. WIELAND,† AND A. M. SCHEIDEGGER†,‡

Paul Scherrer Institute, Laboratory for Waste Management, 5232 Villigen PSI, Switzerland, and Department of Environmental Sciences, Swiss Federal Institute of Technology (ETH), Zürich, Switzerland

Cement-based materials play an important role in multibarrier concepts developed worldwide for the safe disposal of hazardous and radioactive wastes. Cement is used to condition and stabilize the waste materials and to construct the engineered barrier systems (container, backfill, and liner materials) of repositories for radioactive waste. In this study, Ni uptake by hardened cement paste has been investigated with the aim of improving our understanding of the immobilization process of heavy metals in cement on the molecular level. X-ray absorption spectroscopy (XAS) coupled with diffuse reflectance spectroscopy (DRS) techniques were used to determine the local environment of Ni in cement systems. The Ni-doped samples were prepared at two different water/cement ratios (0.4, 1.3) and different hydration times (1 hour to 1 year) using a sulfate-resisting Portland cement. The metal loadings and the metal salts added to the system were varied (50 up to 5000 mg/kg; NO_3^-, SO_4^{2-}, Cl^-). The XAS study showed that for all investigated systems Ni(II) is predominantly immobilized in a layered double hydroxide (LDH) phase, which was corroborated by DRS measurements. Only a minor extent of Ni(II) precipitates as Ni−hydroxides (α-$Ni(OH)_2$ and β-$Ni(OH)_2$). This finding suggests that Ni−Al LDH, rather than Ni−hydroxides, is the solubility-limiting phase in the Ni-doped cement system.

Introduction

Assuring safe disposal and long-term storage of hazardous and radioactive wastes represents a primary environmental task of industrial societies. The long-term disposal of the hazardous waste is associated with landfilling of cement-stabilized waste (*1*), whereas deep geological disposal is foreseen for some categories of cement-stabilized radioactive waste (*2*). For example, more than 90 wt% of the near-field material of the planned Swiss geological repository for intermediate-level waste consists of hardened cement paste (HCP) and cementitious backfill materials. The HCP is used to solidify the radioactive waste. For this reason, an understanding of the immobilization processes within a hydrating cement is essential to predict the long-term fate of contaminants in the geosphere. From a chemical standpoint, HCP is a very heterogeneous material with discrete particles in the nano- to micrometer size range. The material consists of mainly calcium (aluminum) silicate hydrates, portlandite (calcium hydroxide), and calcium aluminates. The immobilization potential of HCP originates from its selective binding properties for metal cations and anions (*3*). Thus, it appears that immobilization processes in cement systems are highly specific with respect to the mineral components and mechanisms involved.

Ni is among the most important contaminant in waste materials resulting from a variety of industrial processes. For example, Ni radioisotopes associated with irradiated metallic components from nuclear power plants are present in cement-stabilized radioactive waste. In this case, this information is of major importance for predicting the long-term fate of Ni in the cementitious matrix of a disposal site. In connection with the disposal of non-radioactive waste, molecular level information will allow more detailed assessment of the leachability of heavy metals, for example, Ni, from landfills into the environment. Earlier experiments on the Ni uptake by blended and Portland cement indicated that, under highly alkaline conditions (pH > 12.5), poorly crystalline $Ni(OH)_2$ (*4*) and Ni−Al layered double hydroxide (Ni−Al LDH) phases (*5*, *6*) may be formed. LDH phases can be commonly expressed as $[M^{II}_{1-x}M^{III}_x(OH)_2]^{x+}(A^{n-})_{x/n}\cdot yH_2O$, where the M^{II} position can be at least partially filled with Ni, M^{III} position with Al, and the A^{n-} with different anions such as CO_3^{2-}, NO_3^-, Cl^-, and SO_4^{2-}. A natural occurring Ni−Al LDH mineral is Takovite, also named Eardleyit ($Ni_6Al_2(OH)_{16}CO_3\cdot 4H_2O$).

The objective of the present study was to investigate Ni immobilization during cement hydration. The hydration process was started by adding Ni salt solution to the unhydrated cement. The sulfate-resisting Portland cement previously used by Scheidegger et al. (*5*, *6*) was also employed as starting material for the present study. Note that the experimental setup differs from that used in the earlier studies (*5*, *6*) where the Ni uptake by hydrated cement was investigated.

A combination of wet chemistry experiments, X-ray absorption spectroscopy (XAS), and diffuse reflectance spectroscopic (DRS) measurements was used to gain a molecular level understanding of the immobilization processes. The synergistic use of these techniques was expected to provide information on the solubility-limiting phase, chemical speciation, and the structural coordination environment of Ni in hydrated cement.

Materials and Methods

Sample Preparation. The cement samples were prepared from a commercial sulfate-resisting Portland cement (CEM I 52.5 N HTS, Lafarge, France) used to condition radioactive waste in Switzerland. Ni-doped HCP was prepared by mixing different Ni salt solutions (NO_3^-, SO_4^{2-}, Cl^-) with unhydrated cement. The metal salts were dissolved in deionized water to obtain stock solutions with concentrations of 0.3, 0.03, and 0.003 mol/L (pH = 4.5−5). The solutions were mixed with the unhydrated cement at two different water/cement (w/c) ratios (0.4, 1.3) using a standard procedure (*7*). The degree of hydration is enhanced with increasing w/c ratio (*8*). The final metal concentrations of the pastes were 50, 500, and 5000 mg/kg dry (Table 1). The cement pastes were placed into Plexiglas moulds, which were closed with polyethylene lids, and hydrated between 1 hour and ~1 year. For short hydration times up to 6 hours, the slurries were filtered (0.2 μm pore size) to separate the solid from the free

* Corresponding author phone: +41-56-310-2966; fax: +41-56-310-4595; e-mail: marika.vespa@psi.ch.
† Paul Scherrer Institute.
‡ Swiss Federal Institute of Technology (ETH).

10.1021/es052240q CCC: $33.50
Published on Web 03/02/2006

TABLE 1. Experimental Parameters for the Ni-Doped HCP Samples

sample name	salt	initial Ni concentration in solution (M)	w/c[a]	target metal concentration in HCP (mg/kg)	hydration time
Ni_cem_1h	$Ni(NO_3)_2$	0.3	0.4	5000	1 hour
Ni_cem_6h	$Ni(NO_3)_2$	0.3	0.4	5000	6 hours
Ni_cem_3d	$Ni(NO_3)_2$	0.3	0.4	5000	3 days
Ni_cem_30d	$Ni(NO_3)_2$	0.3	0.4	5000	30 days
Ni_cem_150d	$Ni(NO_3)_2$	0.3	0.4	5000	150 days
Ni_cem_1y	$Ni(NO_3)_2$	0.3	0.4	5000	1 year
Ni_cem_500	$Ni(NO_3)_2$	0.03	0.4	500	30 days
Ni_cem_50	$Ni(NO_3)_2$	0.003	0.4	50	30 days
Ni_cem_w/c_1.3	$Ni(NO_3)_2$	0.3	1.3	5000	30 days
Ni_cem_Cl	$NiCl_2$	0.3	0.4	5000	30 days
Ni_cem_SO_4	$Ni(SO_4)$	0.3	0.4	5000	30 days

[a] w/c = water/cement ratio.

water. The solid materials were washed with acetone for 15 min to stop the hydration process (*8*), filtered, and dried in a glovebox under controlled N_2 atmosphere (CO_2, O_2 < 2 ppm, $T = 20 \pm 3$ °C). The samples hydrated for longer time periods were stored in closed containers at 100% relative humidity. The cylinders were cut into several slices of ~1 cm thickness and dried in the glovebox. Some slices were crushed to obtain size fractions <100 μm using a tungsten/carbide pebble mill. The powder material was employed for extended X-ray absorption fine structure (EXAFS) and DRS measurements as well as for wet chemistry experiments. For EXAFS measurements, the powder material was placed into Plexiglas holders and sealed with Kapton tape.

Wet Chemistry Experiments. The wet chemistry experiments were conducted using Ni-doped HCP samples reacted for 30 days with Ni loadings of 5000 mg/kg (Ni_cem_30d) and 500 mg/kg (Ni_cem_500, Table 1). Prior to use in the wet chemistry experiments, the HCP material was crushed and sieved to collect the size fraction of <63 μm. The material was mixed with artificial cement pore water (ACW) at a solid/liquid (S/L) ratio of 5 g/L and shaken end-over-end for 1, 14, 30, and 60 days in the glovebox under controlled N_2 atmosphere. After equilibration, solid and liquid phases were separated by centrifugation (60 min at 95 000*g*). Aliquots were withdrawn from the supernatant solution to determine the Ni concentration using inductively coupled plasma mass spectroscopy (ICP-MS, detection limit = 0.05 μg/L). Prior to the ICP-MS measurements, the concentration of the main elements (Na, K, Ca) was determined using inductively coupled plasma optical emission spectroscopy (ICP-OES) to take into account matrix effects.

The composition of ACW corresponds to the chemical composition of a solution in equilibrium with a freshly prepared HCP (*8*). Under these conditions, the ACW is a (Na,K)OH rich fluid saturated with respect to portlandite and calcite (pH = 13.3). The basic preparation and the chemical composition of ACW are described elsewhere (*9*, *10*).

EXAFS Data Collection and Reduction. EXAFS spectra at the Ni K-edge were collected at the Swiss Norwegian Beam Line (SNBL) and at the Dutch Belgium Beamline (DUBBLE) at the European Synchrotron Radiation Facility (ESRF) in Grenoble, France. Both beamlines are equipped with a Si(111) crystal monochromator. The measurements were collected at room temperature in transmission (ionization chambers) and in fluorescence mode (SNBL, Lytle detector; DUBBLE, 9 channel monolithic Ge-solid-state detector). The monochromator angle was calibrated by assigning the energy of 8333 eV to the first inflection point of the K-absorption edge spectrum of Ni metal foil.

EXAFS data reduction was performed using the WinXAS 3.1 software package following standard procedures (*11*). The energy was converted to photoelectron wave vector units ($Å^{-1}$) by assigning the origin E_0 to the first inflection point of the absorption edge. Radial structure functions (RSF) were obtained by Fourier transforming the k^3-weighted $\chi(k)$ functions between 3.2 and 10.9 $Å^{-1}$ with a Bessel window function with a smoothing parameter of 4. Multishell fits were performed in real space across the range of the first two shells ($\Delta R = 0.8-3.5$ Å). Theoretical scattering paths for the fit were calculated using FEFF 8.2 (*12*) and the structure of β-$Ni(OH)_2$ as a reference. The amplitude reduction factor (S_0^2) was determined to be 0.85 from the experimental β-$Ni(OH)_2$ EXAFS spectrum (*5*). Errors on the structural parameters were estimated from the analysis of a series of reference compounds (β-$Ni(OH)_2$, α-$Ni(OH)_2$; see Table 2). Several reference spectra (β-$Ni(OH)_2$, α-$Ni(OH)_2$, synthetic Ni−Al LDH (Ni:Al, 2:1; $Ni_2Al(OH)_6(CO_3)_{1/2}$ (*13*)), Ni-phyllosilicate (*14*), neo-formed Ni−Al LDH formed from Ni-doped pyrophyllite (*15*)) were used in support of the identification of the Ni speciation in the cement matrix.

Wavelet transform analysis (WT) of EXAFS spectra was used to complement the Fourier transform. WT enables a 2D visualization of the Fourier transform, with resolution in both k ($Å^{-1}$) and R space (Å) (*16*, *17*). WT allows atoms to be distinguish, which are located at the same distance R but yield contributions at different k ranges. Recently, Muñoz et al. (*17*) applied a continuous Cauchy WT to simultaneously decompose the EXAFS spectra of geochemical and environmental materials in reciprocal and real space. In a similar manner, Funke et al. (*16*) applied the Morlet wavelet to resolve the short-range structure of Zn−Al LDH. The Morlet WT allows the optimization of the parameters η and σ. The frequency of the sine and cosine functions, η, determines how many oscillations of the sine wave are covered by a Gaussian envelope with the half-width $\sigma = 1$. Funke et al. (*16*) demonstrated that the optimum resolution at a given distance (r_{opt}) of interest is achieved by $\eta_{opt} \cong 2r_{opt}$ for $\sigma = 1$.

Diffuse Reflectance Spectroscopy (DRS). DRS has been used in the past to study Ni and other transitional metals in catalysis (*18*) and in environmental science (*19*, *20*). The information provided by DRS is related to the local symmetry of the first coordination shell. For example, DRS is more sensitive to relative changes in the Ni−O distance than EXAFS. Scheinost et al. (*19*) showed the potential of DRS in identifying different Ni phases based on the energy position of the $\nu 2$ band. This band corresponds to the $^3A_{2g} \rightarrow {}^3T_{1g}$ transition of the crystal field.

In this study ,the DRS experiments were conducted using a Varian Cary 5 UV−Vis−NIR spectrophotometer described elsewhere (*21*). White reflectance standard $BaSO_4$ (Kodak) was used to record the baseline. Processing of the spectra included subtraction of the baseline and calculation of the

TABLE 2. Structural Information Obtained from EXAFS Ni K-edge Data Analysis[a]

	Ni−O			Ni−Ni			Ni−Si				
samples	CN	R (Å)	σ^2 (Å^2)	CN	R (Å)	σ^2 (Å^2)	CN	R (Å)	σ^2 (Å^2)	ΔE_0 (eV)	res%
references											
Ni-phyllosilicate[b]	5.1	2.04	0.006	3.5	3.07	0.008[d]	3.7	3.26	0.008[d]	0.3	3.0
β-Ni(OH)$_2$	5.6	2.06	0.005	5.6	3.13	0.005				−0.6	3.0
α-Ni(OH)$_2$	5.2	2.03	0.005	4.9	3.09	0.005[e]				3.0	4.4
Ni−Al LDH (LDH)	6.0	2.05	0.006	2.5	3.06	0.005[e]				1.1	4.5
neo-formed Ni−Al LDH[c] (N-LDH)	5.7	2.04	0.004	3.9	3.07	0.005[e]				0.3	3.8
cement samples											
Ni_cem_1h	4.9	2.04	0.005	3.8	3.09	0.005[e]				−0.7	4.4
Ni_cem_6h	4.9	2.03	0.004	3.8	3.08	0.005[e]				−2.4	4.3
Ni_cem_3d	6.9	2.05	0.008	3.2	3.10	0.005[e]				0.0	7.6
Ni_cem_30d	7.3	2.05	0.007	3.0	3.11	0.005[e]				1.3	7.9
Ni_cem_150d	5.9	2.04	0.005	2.9	3.09	0.005[e]				−1.7	2.9
Ni_cem_1y	6.5	2.04	0.006	3.0	3.09	0.005[e]				−1.8	4.1
Ni_cem_500	5.3	2.05	0.005[e]	2.3	3.12	0.005[e]				0.0	9.0
Ni_cem_50	6.3	2.04	0.005[e]	1.8	3.17	0.005[e]				−0.3	10.8
Ni_cem_w/c_1.3	5.5	2.05	0.004	3.0	3.10	0.005[e]				−0.9	4.3
Ni_cem_Cl	5.0	2.04	0.004	2.9	3.10	0.005[e]				−0.5	3.5
Ni_cem_SO$_4$	6.4	2.05	0.007	2.7	3.08	0.005[e]				−0.7	4.0

[a] CN, R, σ^2, and ΔE_0 stand for coordination number, interatomic distance, Debye−Waller factor, and inner potential correction. Estimated errors: $R_{(Ni-O)} \pm 0.02$ Å, $CN_{(Ni-O)} \pm 0.02$ Å, $CN_{(Ni-Ni)} \pm 20\%$. res% = deviation between experimental data and fit given by the relative residual in percent. N = number of data points. y_{exp} and y_{theo} = experimental and theoretical data points, respectively. $\%res = ((\sum_{i=1}^{N} |y_{exp}(i) - y_{theo}(i)|)/(\sum_{i=1}^{N} y_{exp}(i)))*100$. [b] Dähn et al., 2002. [c] Scheidegger et al., 1997. [d] Correlated parameters. [e] Fixed parameters during fitting procedures.

Kubulka−Munk function. Blanks, that is, samples prepared in the same way as the Ni-doped HCP samples but without metal addition, were used for spectral background subtraction. The spectra of reference compounds (synthetic Ni−Al LDH (Ni:Al, 2:1), commercial Ni(NO$_3$)$_2$, and β-Ni(OH)$_2$) were also recorded at the same time.

Results and Discussion

Wet Chemistry Data. Wet chemistry experiments were carried out to quantify the Ni partition between the Ni-doped HCP and ACW, and compare the results with earlier measurements of the Ni sorption isotherm on HCP prepared from the same type of cement (*10*). Wet chemistry data allow first assessments of the binding mechanism of Ni in the cement matrix to be made. In this study, the Ni partition between the Ni-doped HCP samples with Ni loadings of 5000 mg/kg dry HCP (Ni_cem_30d) and 500 mg/kg dry HCP (Ni_cem_500) was determined after 30 days equilibration of the suspensions. Preliminary kinetic tests over the time period of 60 days revealed that 7 days equilibration was the minimum time required to achieve constant Ni concentrations in solution (data not shown). Nevertheless, 30 days equilibration was chosen to allow direct comparison of the aqueous Ni concentrations in these systems with the concentration measurements reported by Wieland et al. (*10*).

Figure 1 shows the Ni concentration in solution upon equilibration of the Ni_cem_30d and Ni_cem_500 sample material in ACW together with the sorption isotherm data reported in Wieland et al. (*10*). The figure reveals that the trend to increasing aqueous Ni concentrations with increasing Ni loadings is comparable in both systems. Thus, similar Ni concentrations are determined regardless of the initial Ni source, that is, whether Ni was released from the Ni-doped HCP or added to solution and subsequently sorbed onto HCP. As discussed by Wieland et al. (*10*), the Ni concentration in ACW lies above the Ni concentration of pristine HCP equilibrated in ACW and below the solubility of β-Ni(OH)$_2$, indicating that the solubility-limiting phase is not β-Ni(OH)$_2$. It should be noted that for the experimental setup used in the present study (adding a highly concentrated Ni solution to the alkaline cement system) and based on the available thermodynamic data (ref *22* and therein), β-Ni(OH)$_2$ was

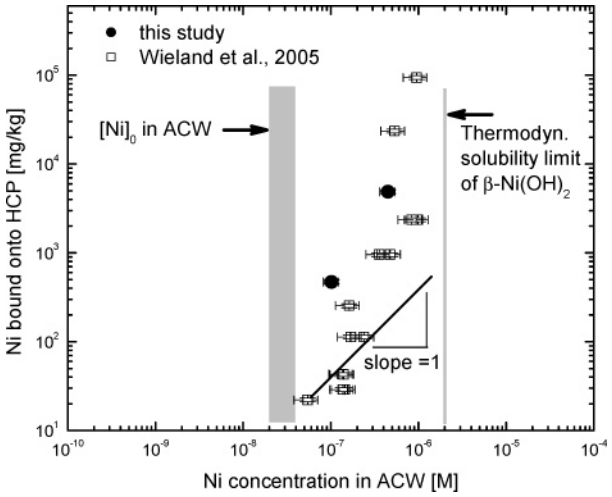

FIGURE 1. The concentration of Ni taken up by HCP shown as a function of the concentration of dissolved Ni in ACW (pH = 13.3). ●, 5000 and 500 mg/kg metal loading (this study); □, data from Wieland et al. (*10*). All samples were equilibrated for 30 days. The shaded area indicates the Ni concentration in ACW; the gray line indicates the solubility limit of β-Ni(OH)$_2$.

expected to be the only Ni phase formed during cement hydration. The good agreement of the wet chemistry data obtained in this study and those reported by Wieland et al. (*10*) suggests that the same mechanism might be responsible for the Ni uptake by HCP regardless of the different methods used for the sample preparation. It is worth emphasizing that, in contrast to the earlier studies (*5*, *6*, *10*), in the present study Ni was taken up by the cement matrix during the hydration process. Wieland et al. (*10*) concluded that the Ni immobilization by HCP could not be interpreted in terms of an adsorption-type process. The authors rather suggested that the Ni concentration in solution is controlled by a solubility-limiting process due to the formation of a solid phase with varying composition (solid solution). This finding is further supported by the spectroscopic studies of Scheidegger et al. (*5*, *6*), which suggested that a Ni−Al LDH-type phase is the solubility-limiting phase.

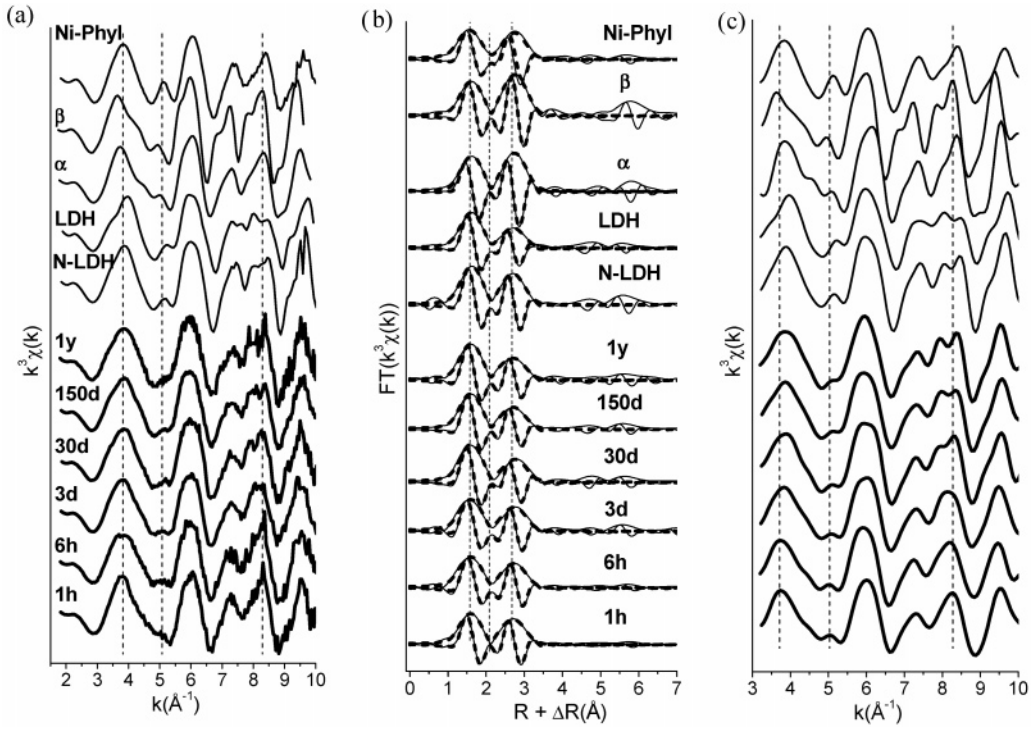

FIGURE 2. Experimental spectra of Ni-reference compounds and Ni-doped HCP samples with 5000 mg/kg Ni concentration and hydrated between 1 hour and 1 year: (a) k^3-weighted, normalized, background-subtracted EXAFS spectra, (b) experimental (solid line) and theoretical (dashed line) Fourier transforms (modulus and imaginary parts) obtained from the EXAFS spectra presented in Figure 2a, and (c) k^3-weighted EXAFS function for the Fourier-backtransform spectra obtained from Figure 2b (range: $R + \Delta R = 0.8-7$ Å). Dashed lines indicate spectral features explained in detail in the text. N-LDH = neo-formed Ni−Al LDH (*15*), LDH = synthetic Ni−Al LDH (Ni:Al, 2:1) (13), α = α-$Ni(OH)_2$, β = β-$Ni(OH)_2$, Ni-phyl = Ni-phyllosilicate (*14*).

Formation of a Ni−Al LDH Phase. Figure 2a shows the normalized, background-subtracted, and k^3-weighted EXAFS spectra of HCP samples with Ni loadings of 5000 mg/kg and hydrated for different times together with relevant reference spectra (Table 1). For the following discussion, samples with hydration times longer than 30 days (Ni_cem_30d, Ni_cem_150d, Ni_cem_1y) will be considered.

Figure 2a reveals that the first oscillation at ~4 $Å^{-1}$ of the experimental spectra is at a position similar to that of the neo-formed LDH phase, which forms upon Ni uptake by pyrophyllite (N-LDH) (*15*). The experimental spectra show a small feature at ~5 $Å^{-1}$ on the left side of the oscillation at 6 $Å^{-1}$, which is well reproduced in both synthetic and neo-formed Ni−Al LDH spectra. The amplitude of this spectral feature is clearly damped as compared to the Ni-phyllosilicate spectrum. The beat pattern at ~8 $Å^{-1}$ of the Ni-doped HCP samples shows a splitting of the oscillation. Scheinost and Sparks (*23*) demonstrated that the beat pattern at ~8 $Å^{-1}$ suggests the presence of Ni−Al LDH. In fact, this beat pattern is observed in both Ni−Al LDH spectra, whereas the other reference compounds (α-$Ni(OH)_2$, β-$Ni(OH)_2$, and Ni-phyllosilicate) show an elongated upward oscillation ending in a sharp tip at ~8 $Å^{-1}$. Thus, the presence of the beat pattern at ~8 $Å^{-1}$ together with the observed spectral features at ~4 and ~5 $Å^{-1}$ indicate that a Ni−Al LDH phase has formed in Ni-doped HCP samples.

The corresponding Fourier transforms (FT) of the k^3-weighted EXAFS spectra are shown in Figure 2b. The amplitude of the first peak ($R + \Delta R$ = ~1.6 Å) is similar for all samples and references. The imaginary part of the FT spectra of the Ni-doped HCP samples at $R + \Delta R$ = ~2 Å shows similarities to the α-$Ni(OH)_2$ and Ni−Al LDH reference compounds. The position of the second peak of the samples hydrated for 150 days (Ni_cem_150d) and for 1 year (Ni_cem_1y) is slightly shifted to lower values ($R + \Delta R$ = ~2.71 Å) as compared to the sample hydrated for 30 days (Ni_cem_30d) ($R + \Delta R$ = ~2.78 Å). The latter distance is comparable to those determined for the β-$Ni(OH)_2$ and Ni-phyllosilicate reference compounds ($R + \Delta R$ = ~2.75 Å). However, the shorter distance corresponds to those determined for α-$Ni(OH)_2$ or Ni−Al LDH, respectively ($R + \Delta R$ = ~2.71 Å). The amplitude of the second peak in the experimental spectra of all Ni-doped HCP samples and the Ni−Al LDH reference compounds is clearly reduced as compared to the other samples, supporting the presence of Ni−Al LDH in the cement samples.

The structural parameters derived from multi-shell analysis (ΔR = 0.8−3.5 Å) are summarized in Table 2. The first coordination shell was fitted with Ni−O backscattering pairs. The second coordination shell was fitted solely using Ni−Ni pairs, because the discrimination of Ni−Ni and Ni−Al backscattering pairs in Ni−Al LDH is problematic (*5*, *6*). To be able to compare the coordination numbers of the Ni−Ni backscattering pairs (CN_{Ni-Ni}) of all samples and references, the Debye−Waller factor was fixed to 0.005 $Å^2$ as determined for the β-$Ni(OH)_2$. Data analysis reveals similar CN and interatomic distances (R) for all cement samples (Table 2). The first FT peak corresponds to an octahedral coordination of Ni with ~6 oxygen atoms at 2.04−2.05 Å. The CN_{Ni-Ni} (~3) are strongly reduced as compared to α-$Ni(OH)_2$ and β-$Ni(OH)_2$. However, the CN_{Ni-Ni} of the HCP samples are similar to that determined for Ni−Al LDH. The CN_{Ni-Ni} is reduced as Ni is partly substituted by Al in Ni−Al LDH, resulting in a significant destructive interference between Ni and Al backscattering contributions and causing an amplitude cancellation of the Ni and Al shells (*6*, *14*). The CN_{Ni-Ni} in β-$Ni(OH)_2$ is close to 6 as expected from literature data (*24*), whereas the CN_{Ni-Ni} of α-$Ni(OH)_2$ is slightly lower (4.9). The difference in the CN is attributed to Ni vacancies in the brucite-like $Ni(OH)_2$ layer (*25*).

Although the CN_{Ni-Ni} of the Ni-doped HCP samples and Ni−Al LDH agree very well, the overall Ni−Ni distances of

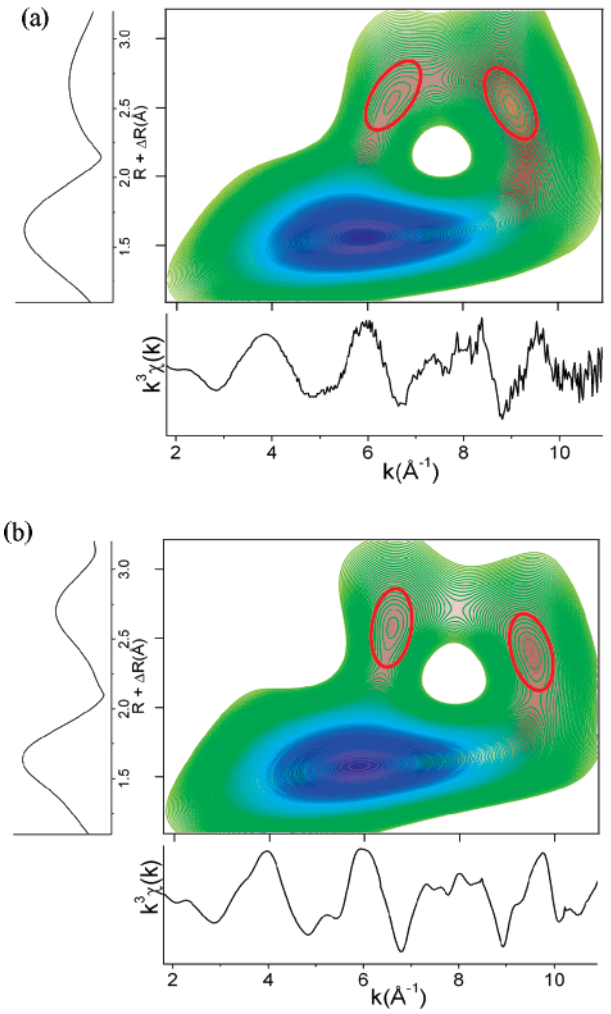

FIGURE 3. Wavelet analysis of the first and second shell ($\eta = 5.7$, $\sigma = 1$, (*16*)) of (a) Ni_cem_1y sample (5000 mg/kg Ni loading, hydrated for 1 year), and (b) Ni−Al LDH synthetic reference compound (LDH, Ni:Al, 2:1) (13). Circled areas indicate contributions of Ni−Ni and Ni−Al backscattering pairs. Note the slight difference in *R* between the experimental spectrum and the reference compound for the maxima at $k = \sim 6.6$ Å^{-1} and ~ 9.2 Å^{-1}. This is due to the fact that the experimental spectrum is composed of a mixture of Ni−Al LDH and Ni−hydroxide phases, and not of a pure Ni−Al LDH, as for the reference compound. The Ni−hydroxide phases cause the R_{Ni-Ni} to shift to slightly longer distances *R*.

the HCP samples are longer (R_{Ni-Ni} = 3.09−3.11 Å) as compared to 3.06−3.07 Å (Ni−Al LDH). This finding suggests that, in addition to Ni−Al LDH phase, other Ni-containing phases form. The longer R_{Ni-Ni} is attributed to the presence of β-Ni(OH)$_2$ impurities (R_{Ni-Ni} = 3.13 Å). β-Ni(OH)$_2$ is expected to form because the Ni solution used for the sample preparation is strongly oversaturated with respect to Ni−hydroxide upon contact with cement (pH of the pore solution ~12.8−13.3).

The presence of Ni−Ni and Ni−Al backscattering contributions is further substantiated using WT analysis. Figure 3 shows the WT of the sample hydrated for 1 year (Ni_cem_1y) (Figure 3a) and the synthetic Ni−Al LDH (Figure 3b), which were deduced using the optimized Morlet parameters η = 5.7 and $\sigma = 1$, and a k^3-weighted signal. Both samples show a maximum at $R + \Delta R = \sim 1.6$ Å and at $k = \sim 6$ Å^{-1} with a contribution in k-space ranging between ~2 and ~9 Å^{-1}. This corresponds to the first metal shell (Ni−O). The WT of both samples resolves two maxima at $k = \sim 6.6$ Å^{-1} and $k = \sim 9.2$ Å^{-1} for the peak at $R + \Delta R = \sim 2.7$ Å, respectively. Thus,

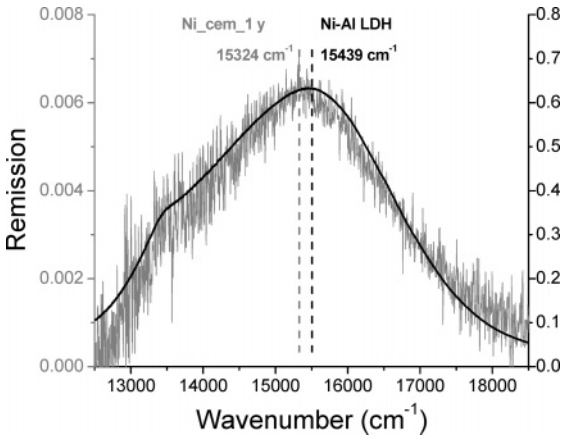

FIGURE 4. DRS measurement of Ni_cem_1y sample (gray) (5000 mg/kg Ni loading, hydrated for 1 year) and Ni−Al LDH synthetic reference compound (black) (LDH, Ni:Al, 2:1) (13). Note the different ordinates used for Ni_cem_1y (gray, left) and for Ni−Al LDH (black, right) and that the noise level of the Ni_cem_1y sample is higher as compared to the reference due to lower Ni−Al LDH concentration.

based on the similarities of the WT, we infer that the second peak in the FT of the Ni-doped HCP sample and Ni−Al LDH consists of two identical contributions, resulting from Ni−Ni and Ni−Al backscattering pairs. This finding supports our hypothesis that Ni−Al LDH is formed in the cement samples.

Independent evidence of the Ni−Al LDH formation in Ni-doped HCP samples was further obtained from DRS measurements. Figure 4 shows the DRS measurements for the sample hydrated for 1 year (Ni_cem_1y) and the synthetic Ni−Al LDH. The Ni−Al LDH has a $\nu 2$ band position at 15 439 cm^{-1}, which is comparable to the position reported by Scheinost et al. (*19*) (15 220 cm^{-1} − 15 430 cm^{-1}), and a small shoulder at 13 480 cm^{-1}. The Ni_cem_1y sample shows a $\nu 2$ band position at 15 324 cm^{-1} and a small shoulder at ~13 500 cm^{-1}, which is in good agreement with the reference compound. This indicates that predominantly Ni−Al LDH has formed in the cement sample.

Time Dependency of the Ni−Al LDH Formation. Samples with hydration times varying between 1 hour and 1 year were investigated to assess the influence of the hydration time on Ni binding in hydrated cement. Figure 2a shows the normalized, background-subtracted, and k^3-weighted EXAFS spectra of Ni-doped HCP samples hydrated up to 1 year. In all experimental spectra, the spectral features at ~4, ~5, and ~8 Å^{-1} appear. The oscillation at ~4 Å^{-1} becomes broader with increasing hydration time. The position of this oscillation for the short hydration times (1 and 6 hours; Ni_cem_1h and Ni_cem_6h) is comparable to that of the Ni−hydroxide phases (Figure 2a). In contrast, the position of this oscillation in the longer hydrated samples (3 days up to 1 year; Ni_cem_3d−Ni_cem_1y) corresponds to that of Ni−Al LDH. Furthermore, the right shoulder of this oscillation for the short hydration times (Ni_cem_1h and Ni_cem_6h) shows a small feature similar to α-Ni(OH)$_2$. The spectral feature detected at ~5 Å^{-1} shifts slightly to the right (dashed line) with increasing hydration time. The oscillation at ~8 Å^{-1} shows an elongated upward oscillation ending at ~8.5 Å^{-1} for the Ni_cem_1h and Ni_cem_6h samples, similar to α-Ni(OH)$_2$ (Figure 2a). The EXAFS spectra of the Ni-doped HCP samples with hydration times longer than 3 days show a splitting of the oscillation at ~8 Å^{-1}. The three spectral features (~4, ~5, ~8 Å^{-1}) are better visualized in the Fourier-backtransform (FT^{-1}) shown in Figure 2c (ΔR = 0.8−7 Å). The broadening of the feature at ~4 Å^{-1}, the shift of the feature at ~5 Å^{-1}, and the splitting of the oscillation at ~8 Å^{-1} indicate that the portion of Ni−Al LDH formed in HCP increases with increasing

hydration time. At short hydration times, however, the slight shift of the feature at ~4 Å^{-1} and the shoulder of the feature at ~4 Å^{-1} suggest that the spectra of the Ni-doped HCP samples are very similar to those of the Ni−hydroxide phases.

The corresponding FT of the k^3-weighted EXAFS spectra (Figure 2b) shows no evident dependence on the hydration time. Data analysis reveals similar Ni−O and Ni−Ni distances for all Ni-doped HCP samples. However, the CN_{Ni-Ni} decreases from 3.8 to 3.0 with increasing hydration time (Table 2). This decrease in the CN_{Ni-Ni} is caused by destructive interference of Ni−Ni and Ni−Al backscattering pairs as discussed earlier. The finding of a significant reduction of CN_{Ni-Ni} indicates substantial substitution of Ni by Al.

To test whether a mineral mixture would be consistent with the observed spectra, the EXAFS spectra of the Ni-doped HCP samples were fitted with linear combinations of α-$Ni(OH)_2$, β-$Ni(OH)_2$, and Ni−Al LDH. The amount of Ni−Al LDH in the Ni-doped HCP samples was found to increase with increasing hydration time (from ~40% to ~60%), whereas α-$Ni(OH)_2$ decreases accordingly (from ~35% to ~20%). Finally, the content of β-$Ni(OH)_2$ was found to be small (~20%) and remained constant with time.

Influence of Other Experimental Parameters. Besides hydration time, other experimental parameters were expected to have a potential effect on the Ni speciation, for example, the initial Ni concentrations, the anions added to the system, and the w/c ratio. Therefore, these parameters were varied to assess their influence on the Ni uptake by hydrating cement.

Figure 5 shows the normalized, background-subtracted, and k^3-weighted EXAFS spectra (a), the FT (b), and the FT^{-1} (c) of Ni-doped HCP samples hydrated for 30 days. These samples were either doped with $Ni(NO_3)_2$ at different concentrations (50, 500, 5000 mg/kg; Ni_cem_50, Ni_cem_500, Ni_cem_30d) and different w/c ratios (0.4 and 1.3; Ni_cem_30d, Ni_cem_w/c_1.3), or the Ni salts used for the sample preparation were varied (NO_3^-, SO_4^{2-}, Cl^-; Ni_cem_30d, Ni_cem_SO_4, Ni_cem_Cl) (Table 1). Figure 5a reveals that, for the Ni_cem_SO_4, Ni_cem_Cl, and Ni_cem_w/c_1.3 samples, the oscillations at ~4, ~5, and ~8 Å^{-1} are comparable to those previously observed for the Ni_cem_30d sample, which was prepared at w/c = 0.4 to obtain 5000 mg/kg Ni loading using $Ni(NO_3)_2$. Further, the derived FT of the k^3-weighted EXAFS spectra of these samples shows no noticeable difference from the Ni_cem_30d sample (Figure 5b). To better visualize the contributions resulting from the second shell, a FT^{-1} was performed in the range between 2.2 and 3.40 Å (Figure 5d). The contributions of the second shell in the Ni_cem_SO_4, Ni_cem_Cl, and Ni_cem_w/c_1.3 samples are very similar to that in the Ni_cem_30d sample. Thus, neither the w/c ratios nor the type of anions used for the preparation have any noticeable influence on the EXAFS spectra.

However, some changes in the EXAFS spectra appear at decreasing Ni concentration. The oscillation at ~4 Å^{-1} shows a splitting, which becomes more pronounced in the sample with Ni loading of 50 mg/kg (Ni_cem_50). The oscillation at ~5 Å^{-1} as well as the feature between ~7 and ~8 Å^{-1} diminish with decreasing Ni loading. The described spectral features (~4, ~5, and ~8 Å^{-1}) are better resolved in the FT^{-1} (Figure 5c). The second peak in the FT of the samples with Ni loadings of 500 mg/kg (Ni_cem_500) and 50 mg/kg (Ni_cem_50) shows a shift to the right and a broadening with decreasing Ni concentration as compared to the Ni_cem_30d sample. A FT^{-1} in the range of between 2.2 and 3.40 Å reveals a frequency shift to the left with decreasing Ni concentrations for the Ni_cem_500 and Ni_cem_50 samples, indicating significant changes in the backscattering contributions (Figure 5d).

Structural parameters derived from multi-shell analysis (Table 2) show similar CN_{Ni-O}, CN_{Ni-Ni}, and $R_{Ni-O;Ni-Ni}$ for all

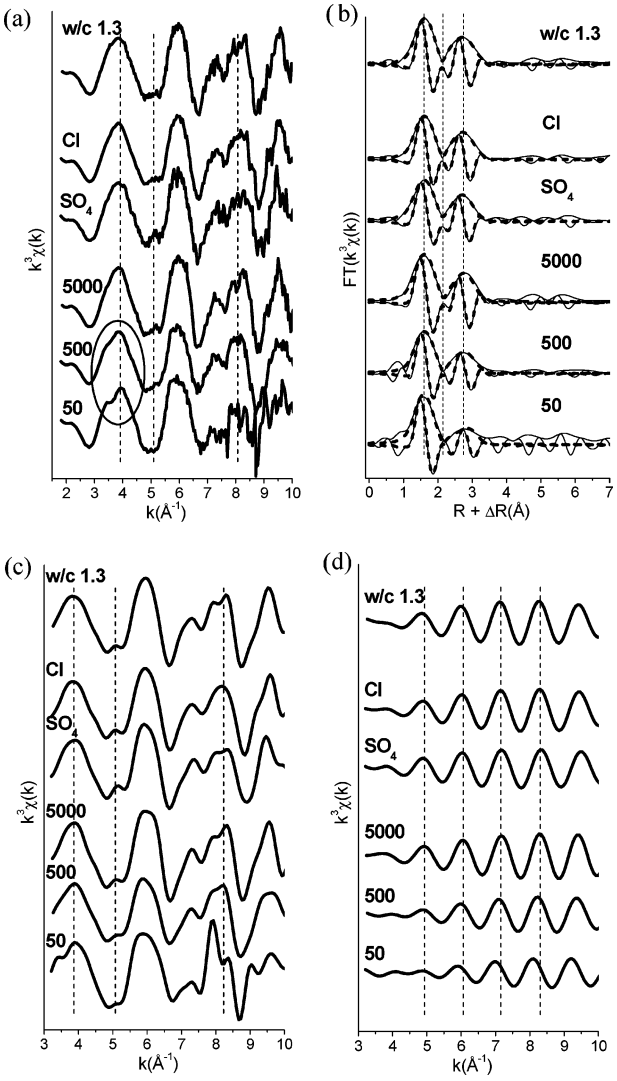

FIGURE 5. Experimental spectra of Ni-doped HCP samples hydrated for 30 days at different concentrations (500, 50), using w/c 1.3 or different anions (Cl^-, SO_4^{2-}) compared to Ni_cem_30d (NO_3^-, 5000 mg/kg, w/c 0.4) of (a) k^3-weighted, normalized, background-subtracted EXAFS spectra (the circled area indicates features explained in the text), (b) experimental (solid line) and theoretical (dashed line) Fourier transforms (modulus and imaginary parts) obtained from the EXAFS spectra presented in Figure 5a, (c) k^3-weighted EXAFS function for the Fourier-backtransform spectra obtained from Figure 5b (range: $R + \Delta R$ = 0.8−7 Å), and (d) k^3-weighted EXAFS function for the Fourier-backtransform spectra of the second shell obtained from Figure 5b (range: $R + \Delta R$ = 2.20−3.40 Å). Dashed lines indicate spectral features explained in detail in the text. 50 = Ni_cem_50, 500 = Ni_cem_500, 5000 = Ni_cem_30d, SO_4^{2-} = Ni_cem_SO_4, Cl^- = Ni_cem_Cl, w/c 1.3 = Ni_cem_w/c_1.3.

experimental spectra, which are further comparable to structural parameters determined for the Ni_cem_30d sample. The only exception is the Ni_cem_50 sample, for which the multi-shell fit approach used throughout this study failed as it resulted in Ni−Ni distances (3.17 Å) longer than any reported distances for Ni compounds (<3.13 Å). At the present time, the situation regarding the Ni speciation at the lowest loading is unclear.

Controlling Uptake Mechanism of Ni in Cement. From the present study, it appears that the formation of the different Ni phases in the Ni-doped HCP samples is controlled by both kinetic and thermodynamic constraints. The EXAFS results show that the formation of Ni−Al LDH, which

immediately starts upon the addition of a Ni solution to unhydrated cement, is a fast process. Nevertheless, the study further shows that, in addition to Ni−Al LDH, α/β $Ni(OH)_2$ form in the initial phase of the hydration process as the system is strongly oversaturated with respect to Ni−hydroxides. The wet chemistry data, however, suggest that β-$Ni(OH)_2$ is not the thermodynamically most stable phase in the systems. The portion of Ni−Al LDH formed increases with increasing hydration time, indicating that Ni−Al LDH is the thermodynamically most stable Ni-containing phase in the cement matrix. The content of β-$Ni(OH)_2$ was found to be small and remained constant with time, suggesting that the transformation of β-$Ni(OH)_2$ to α-$Ni(OH)_2$ or Ni−Al LDH, respectively, is kinetically hindered. By contrast, α-$Ni(OH)_2$ is transformed into Ni−Al LDH with increasing hydration time as revealed from a decrease of the amount of initially formed α-$Ni(OH)_2$ with time. Note that an enhanced stability of Ni−Al LDH over α-$Ni(OH)_2$ in Al-containing hyperalkaline solution was already indicated in the studies of Wang et al. (*26*). The results of the present study further corroborate the findings of Scheidegger et al. (*5*, *6*). These authors reported the formation of predominantly Ni−Al LDH and minor quantities of β-$Ni(OH)_2$ when Ni was sorbed onto hydrated cement and allowed to react for 150 days. The results from this study and the earlier work of Scheidegger et al. (*5*, *6*) clearly show that both modes of Ni immobilization, that is, during cement hydration and due to sorption onto hydrated cement, lead to identical Ni speciations.

The formation of Ni−Al LDH requires that an Al source is available over the entire period of the hydration process. Lothenbach and Wieland (*8*) recently investigated the hydration process of the cement used in the present study. The Al-containing clinker minerals, which slowly dissolve during hydration, are aluminate and ferrite. The most important Al-containing minerals of the modeled hydrate assemblage are ettringite ($Ca_6Al_2(SO_4)_3(OH)_{12}\cdot 26H_2O$; ∼8 wt%), calcium-monocarboaluminate ($3CaO\cdot Al_2O_3\cdot CaCO_3\cdot 11H_2O$; ∼8 wt %), and hydrotalcite (LDH, $[Mg_{1-x}Al_x(OH)_2]^{x+}(A^{n-})_{x/n}\cdot yH_2O$; ∼1.5 wt %). The formation of ettringite is a fast process, which stops after 24 hours when the sulfate source (gypsum) is exhausted. After that the formation of calcium-monocarboaluminate and hydrotalcite starts, and the portion of the hydrates in the cement matrix slowly increases with time (*8*). In this study, the formation of Ni−Al LDH was observed in the first hours of the hydration process, indicating competition between ettringite and Ni−Al LDH for Al. Nevertheless, a significant influence of the competitive reactions on the hydration process can be excluded due to the small amount of Ni−Al LDH formed at the given initial Ni concentrations.

Acknowledgments

The staff of the Swiss-Norwegian Beam Line (SNBL) and the Dutch Belgium Beamline (DUBBLE) at the European Synchrotron Radiation Facility (ESRF) (Grenoble, France) is thanked for experimental assistance during the EXAFS measurements. Thanks are also extended to Dr. E. Curti, D. Kunz, and Dr. M. Harfouche for assistance during the measuring campaigns. Prof. R. A. Schoonheydt and H. Leeman from the Centre of Surface Chemistry and Catalysis faculty in KU-Leuven provided the DRS measurements, and their contribution to this project is gratefully acknowledged. Dr. C. A. Johnson (EAWAG, Switzerland) is warmly thanked for the Ni−Al LDH reference compounds. Gratitude is expressed to Dr. A. Ulrich (EMPA, Switzerland) for the ICP-MS measurements, S. Köchli (PSI) for the ICP-OES measurements, and D. Kunz (PSI) for his contribution to the wet chemistry experiments. Prof. B. Wehrli (EAWAG, Switzerland) is gratefully acknowledged for useful discussion and constructive comments. Partial financial support was provided by the National Cooperative for the Disposal of Radioactive Waste (Nagra), Switzerland.

Supporting Information Available

Figure S1 showing the structural model of Ni−Al LDH, where the edges of the tetrahedra are filled with Ni and Al, and in the interlayer different anions might be present (CO_3^{2-}, NO_3^-, Cl^-, SO_4^{2-}). This material is available free of charge via the Internet at http://pubs.acs.org.

Literature Cited

(1) Schmidt, M.; Beckefeld, P.; Götz, R.; Kamsties, S.; Kretz, C.; Molitor, N.; Neck, U.; Vogel, P. *Reststoff-und Abfallverfestigung. Immobilisierung von Schadstoffen-Recycling-Verbesserung der Deponiefähigkeit*; Expert Verlag: Renningen-Malmsheim, 1995.

(2) Chapman, N.; McCombie, C. *Principles and standards for the disposal of long-lived radioactive wastes*, 1st ed.; Elsevier Science, Ltd.: Oxford, 2003.

(3) Glasser, F. P. In *Chemistry and microstructure of solidified waste forms*; Spence, R. D., Ed.; Lewis Publishers: Boca Raton, FL, 1993.

(4) Atkins, M.; Glasser, F. P.; Moroni, L. P.; Jack, J. J. Thermodynamic modelling of blended cements at elevated temperatures (50 °C to 90 °C). DoE/UMIP/PR/94.011, 1994.

(5) Scheidegger, A.; Wieland, E.; Dähn, R.; Spieler, P. Spectroscopic evidence for the formation of layered Ni−Al double hydroxides in cement. *Environ. Sci. Technol.* **2000**, *34*, 4545−4548.

(6) Scheidegger, A. M.; Wieland, E.; Scheinost, A. C.; Dähn, R.; Tits, J.; Spieler, P. Ni phases formed in cement and cement systems under highly alkaline conditions: An XAFS study. *J. Synchrotron Radiat.* **2001**, *8*, 916−918.

(7) Döhring, L.; Görlich, W.; Rüttener, S.; Schwerzmann, R. Herstellung von homogenen Zementsteinen mit hoher hydraulischer Permeabilität. Nagra NIB 94-29, 1994.

(8) Lothenbach, B.; Wieland, E. A thermodynamic approach to the hydration of sulphate-resisting Portland cement. *Waste Manage.*, in press.

(9) Wieland, E.; Tits, J.; Spieler, P.; Dobler, J. P. Interaction of Eu(III) and Th(IV) with sulphate-resisting Portland cement. *Mater. Res. Soc. Symp. Proc.* **1998**, *506*, 573−578.

(10) Wieland, E.; Tits, J.; Ulrich, A.; Bradbury, M. H. Experimental evidence for solubility limitation of the aqueous Ni(II) concentration and isotopic exchange of ^{63}Ni in cementitious systems. *Radiochim. Acta* **2006**, *94*, 29−36.

(11) Ressler, T. WinXAS: A program for X-ray absorption spectroscopy data analysis under MS-Windows. *J. Synchrotron Radiat.* **1998**, *5*, 118−122.

(12) Rehr, J. J.; Mustre de Leon, J.; Zabinsky, S. I.; Albers, R. C. Theoretical X-ray absorption fine structure standards. *J. Am. Chem. Soc.* **1991**, *113*, 5135−5140.

(13) Johnson, C. A.; Glasser, F. P. Hydrotalcite-like minerals ($M_2Al(OH)_6(CO_3)_{0.5}XH_2O$, where M = Mg, Zn, Co, Ni) in the environment: synthesis, characterization and thermodynamic stability. *Clays Clay Miner.* **2003**, *51*, 1−8.

(14) Dähn, R.; Scheidegger, A. M.; Manceau, A.; Schlegel, M. L.; Baeyens, B.; Bradbury, M. H.; Morales, M. Neoformation of Ni phyllosilicate upon Ni uptake on montmorillonite: A kinetics study by powder and polarized extended X-ray absorption fine structure spectroscopy. *Geochim. Cosmochim. Acta* **2002**, *66*, 2335−2347.

(15) Scheidegger, A. M.; Lamble, G. M.; Sparks, D. L. The kinetics of nickel sorption on phyrophyllite as monitored by X-ray absorption fine structure (XAFS) spectroscopy. *J. Phys. IV* **1997**, *7 (C2)*, 773−775.

(16) Funke, H.; Scheinost, A. C.; Chukalina, M. Wavelet analysis of extended X-ray absorption fine structure data. *Phys. Rev. B* **2005**, *71*, 094110, 1−7.

(17) Muñoz, M.; Argoul, P.; Farges, F. Continuous Couchy wavelet transform analyses of EXAFS spectra: A qualitative approach. *Am. Mineral.* **2003**, *88*, 694−700.

(18) Bensalem, A.; Weckhuysen, B. M.; Schoonheydt, R. A. In situ diffuse reflectance spectroscopy of supported chromium oxide catalysts: Kinetics of the reduction process with carbon monoxide. *J. Phys. Chem. B* **1997**, *101*, 2824−2829.

(19) Scheinost, A. C.; Ford, R. G.; Sparks, D. L. The role of Al in the formation of secondary Ni precipitates on pyrophyllite, gibbsite, talc, and amorphous silica: A DRS study. *Geochim. Cosmochim. Acta* **1999**, *63*, 3193−3203.

(20) Scheckel, K. G.; Sparks, D. L. Kinetics of the formation and dissolution of Ni precipitates in a gibbsite/amorphous silica mixture. *J. Colloid Interface Sci.* **2000**, *229*, 222−229.

(21) Verberckmoes, A. A.; Uytterhoeven, M. G.; Schoonheydt, R. A. Framework and extraframework Co^{2+} in CoAPO-5 by diffuse reflectance spectroscopy. *Zeolites* **1997**, *19*, 180−189.

(22) Hummel, W.; Curti, E. Nickel aqueous speciation and solubility at ambient conditions: A thermodynamic elegy. *Monatsh. Chem.* **2003**, *134*, 941−973.

(23) Scheinost, A. C.; Sparks, D. L. Formation of layered single- and double-metal hydroxide precipitates at the mineral/water interface: A multiple-scattering XAFS analysis. *J. Colloid Interface Sci.* **2000**, *223*, 1−12.

(24) Mansour, A. N.; Melendres, C. A. Analysis of X-ray absorption spectra of some nickel oxycompounds using theoretical standards. *J. Phys. Chem. A* **1998**, *102*, 65−81.

(25) Bode, H.; Dehmelt, K.; Witte, J. Zur Kenntnis der Nickelhydroxidelektrode-I. Über das Nickel (II)-Hydroxidehydrat. *Electrochim. Acta* **1966**, *11*, 1079−1087.

(26) Wang, C. Y.; Zhong, S.; Konstantinov, K.; Walter, G.; Liu, H. K. Structural study of Al-substituted nickel hydroxide. *Solid State Ionics* **2002**, *148*, 503−508.

Received for review November 8, 2005. Revised manuscript received January 25, 2006. Accepted January 30, 2006.

ES052240Q

SUPPORTING INFORMATION FOR

Spectroscopic Investigation of Ni Speciation in Hardened Cement Paste

M. Vespa[1,2]*, R. Dähn[1], D. Grolimund[1], E. Wieland[1], A. M. Scheidegger[1,2]

[1]Paul Scherrer Institute, Laboratory for Waste Management, 5232 Villigen PSI, Switzerland

[2]Departement of Environmental Sciences, Swiss Federal Institute of Technology (ETH), Zürich, Switzerland

Number of pages: 2

Number of Figures: 1

Number of Tables : 0

*Corresponding author.

Phone: +41-56-310-2966

Fax: +41-56-310-4595

E-mail: marika.vespa@psi.ch

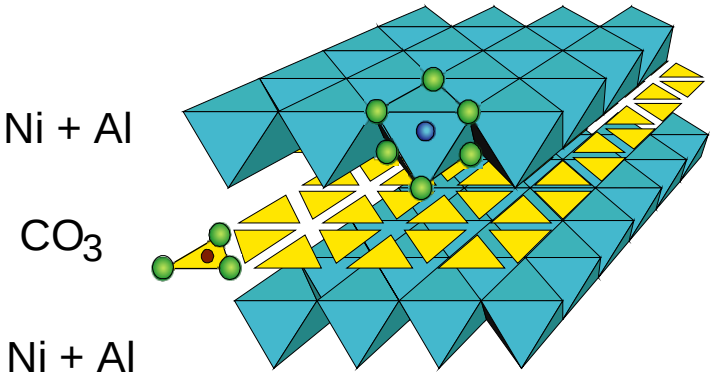

Figure S1. Structural model of Ni-Al LDH. The edge of the tetrahedra are filled with Ni and Al. The interlayer position can be filled with different anions such as CO_3^{2-}, NO_3^-, Cl^-, SO_4^{2-}.